Toward dynamic lumbar punctures guidance based on single element synthetic tracked aperture ultrasound imaging

Haichong K. Zhang, Melissa Lin, Younsu Kim, Mateo Paredes, Karun Kannan, et al.

Haichong K. Zhang, Melissa Lin, Younsu Kim, Mateo Paredes, Karun Kannan, Nisu Patel, Abhay Moghekar, Nicholas J. Durr, Emad M. Boctor, "Toward dynamic lumbar punctures guidance based on single element synthetic tracked aperture ultrasound imaging," Proc. SPIE 10135, Medical Imaging 2017: Image-Guided Procedures, Robotic Interventions, and Modeling, 101350J (3 March 2017); doi: 10.1117/12.2256040

SPIE.

Event: SPIE Medical Imaging, 2017, Orlando, Florida, United States

Toward Dynamic Lumbar Punctures Guidance Based on Single Element Synthetic Tracked Aperture Ultrasound Imaging

Haichong K. Zhang,[a] Melissa Lin,[b] Younsu Kim,[a] Mateo Paredes,[c] Karun Kannan,[c] Nisu Patel,[c] Abhay Moghekar,[d] Nicholas J. Durr,[c] Emad M. Boctor[a,b,d]

[a]Department of Computer Science, [b]Department of Electrical and Computer Engineering, [c]Department of Biomedical Engineering, [d]Department of Neurology, [e]Department of Radiology, The Johns Hopkins University, Baltimore, MD, USA

ABSTRACT

Lumbar punctures (LPs) are interventional procedures used to collect cerebrospinal fluid (CSF), a bodily fluid needed to diagnose central nervous system disorders. Most lumbar punctures are performed blindly without imaging guidance. Because the target window is small, physicians can only accurately palpate the appropriate space about 30% of the time and perform a successful procedure after an average of three attempts. Although various forms of imaging based guidance systems have been developed to aid in this procedure, these systems complicate the procedure by including independent image modalities and requiring image-to-needle registration to guide the needle insertion. Here, we propose a simple and direct needle insertion platform utilizing a single ultrasound element within the needle through dynamic sensing and imaging. The needle-shaped ultrasound transducer can not only sense the distance between the tip and a potential obstacle such as bone, but also visually locate structures by combining transducer location tracking and back projection based tracked synthetic aperture beam-forming algorithm. The concept of the system was validated through simulation first, which revealed the tolerance to realistic error. Then, the initial prototype of the single element transducer was built into a 14G needle, and was mounted on a holster equipped with a rotation tracking encoder. We experimentally evaluated the system using a metal wire phantom mimicking high reflection bone structures and an actual spine bone phantom with both the controlled motion and freehand scanning. An ultrasound image corresponding to the model phantom structure was reconstructed using the beam-forming algorithm, and the resolution was improved compared to without beam-forming. These results demonstrated the proposed system has the potential to be used as an ultrasound imaging system for lumbar puncture procedures.

Keywords: ultrasound imaging, synthetic aperture, lumbar punctures, single element transducer

1. INTRODUCTION

Lumbar punctures (LPs) are performed to collect cerebrospinal fluid (CSF), an important bodily fluid needed to diagnose a variety of central nervous system disorders or conditions, including life threatening ones like meningitis and encephalitis, where a diagnosis delay of a few hours can be catastrophic. More than 400,000 LPs are performed annually, but nearly 23.3% end in failure due to a myriad of challenges [1-2]. These failures lead to misdiagnoses, treatment delays, and subsequent additional unnecessary and dangerous procedures. Patients with excess adipose tissue between skin and target structures, namely obese patients and those with abnormal anatomy (eg: scoliosis, kyphosis), suffer a significantly increased probability of LP failure [3]. The current standard of care utilizes anatomical landmarks to locate the L3-L5 intervertebral space; the needle must be advanced through many tissue layers, between the vertebrae and into the subarachnoid space without hitting other obstacles (e.g. blood vessels or bone) along the way. Most lumbar punctures are performed blindly without the assistance of imaging or guidance mechanisms. Because the target window is small, physicians can only accurately palpate the appropriate space about 30% of the time and perform a successful procedure after an average of three attempts. This results in myriad issues ranging from bloody taps at a 15% incidence rate [4] to post dural puncture headaches (PDPH) induced in 32% of patients [5]. Ultimately, these issues place a costly and uneven burden on both the patient and the healthcare system. The rate of overall complications as a result of lumbar punctures nearly doubles in obese and scoliotic patients at nearly 50% [6-8]. The conventional image guidance in place when a physician is unable to collect CSF with a blind entry is a fluoroscopy. While a fluoroscopy is accurate, it cannot be used on all patients, such as pregnant women, and it is expensive due to the equipment that is necessary and trained

Medical Imaging 2017: Image-Guided Procedures, Robotic Interventions, and Modeling, edited by Robert J. Webster III, Baowei Fei, Proc. of SPIE Vol. 10135, 101350J · © 2017 SPIE
CCC code: 1605-7422/17/$18 · doi: 10.1117/12.2256040

staff (radiologists and radiology technicians). It also delays diagnosis because it is usually scheduled for the following day, and it exposes the patients and physicians to high levels of radiation for the entire duration of the procedure.

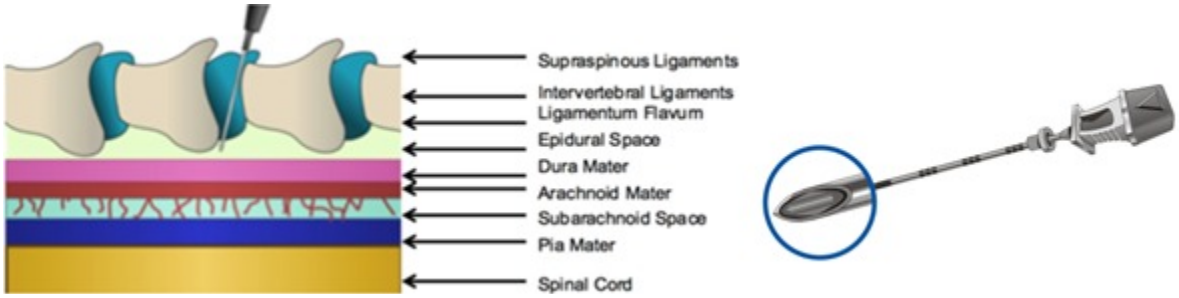

Fig. 1. Illustration of a Quincke needle and its trajectory for lumbar puncture procedures. Left: The layers of tissue from skin to spinal cord; Right: Standard Quincke needle with beveled tip enlarged.

The current state of the art contains solutions that tackle the gaps in the clinical care with regards to needle guidance in the body. A majority of these solutions tackle this issue by improving upon existing imaging technology by introducing tracking methods [9-14]. For example, one solution introduced EM tracking to both the needle and the ultrasound transducer, which resulted in a significant increase in success rate in facet joint injections. However, this technology introduces additional systems to the clinic, which can discourage adoption. Another proposed system was a guidance system that incorporated ultrasound tracking of the needle coupled with patient specific geometries and augmented reality to enable the accurate placement of anesthetic nerve blocks. This approach again forces the physician to familiarize themselves with both the tracking system and augmented reality. Some of the solutions described above have been brought to market. The eZono, eZGuide magnetizes the needle to take advantage of the Hall effect to the track the needle in the body, however this solution does not provide adequate resolution at greater depths. It also introduces a novel system to the clinic which the physician is forced to adapt to. Another example is the ClearGuide One, which utilizes a combination of CT and US to calculate optimal needle trajectory. Much like the eZGuide, ClearGuide fails to provide adequate tracking and image resolution at the needed depths.

A common trait among all existing solutions is the introduction of additional equipment into the procedure creating substantial disruption to existing workflow, which in turn leads to lower adoption rate. With regards to commercial solutions, these solutions are unable to produce high resolution images at the necessary depth where it is most needed. In empirically difficult patients (obese, scoliotic and obstetric), this problem is amplified due to irregular anatomy or a thicker layer of adipose tissue. The limited imaging depth of these techniques have prevented them from being a viable solution for guiding lumbar punctures. The proposed system of this paper aims to leverage the use of the needle, a tool the physician is already familiar with, to introduce an imaging modality to allow for visualization of tissues in lumbar puncture procedures to eliminate failed or traumatic attempts and iatrogenic complications in all patients.

Here, we propose single element Synthetic TRacked AperTure UltraSound (STRATUS) imaging system that provides dynamic image guidance. The system consists of an ultrasound-embedded 14G introducer needle to be used in conjunction with an external holster and back projection based synthetic tracked aperture imaging algorithms to produce high resolution images. In a typical use-case, the physician would insert the needle into the patient subcutaneously and slowly sweep the needle in an arc to acquire an image of the surrounding tissue. This image can then be used to guide and alter the trajectory of the needle to avoid peripheral structures and access the correct target. Once the target is identified, the ultrasound module is removed and a regular small gauge (22, 24 or 26G) needle is placed through the introducer needle to access the dural space. More importantly, the ultrasound scanning and lumbar puncture are two independent procedures and the registration of the image to needle insertion position and angle is crucial. The proposed system utilizes a single ultrasound element that can be inserted below the dermis, and does not require the image-tool registration process.

In this paper, we focus on the proof-of-concept of this technology through simulation and phantom experiments. In simulation, the point targets were imaged for the resolution evaluation, and the tolerances towards various errors have been evaluated. For the experiment, a metal wire phantom mimicking bony structures and actual spine bone phantom were imaged with the controlled motion and freehand scanning. Finally, we discuss the uniqueness compared to other image-guided procedures and the limitation of the system.

2. APPROACH

2.1 Single Element Ultrasound Sensing/Imaging

The concept of the proposed single element Synthetic TRacked AperTure UltraSound (STRATUS) system is shown in Fig. 2(a). The technology consists of two subsystems: the needle-shape ultrasound probe, and the tracking system, which consists of the holster and encoders. The system design includes an insert that can fit inside a Quincke needle. The insert contains a PZT element embedded at the tip, with a magnet wire backing material. The needle is fabricated using a stainless steel tube with a magnet wire threaded through, with one end of the magnet wire connected to the PZT element and the other end soldered to a coaxial cable with a BNC connector. A tracking system is used to track the position of the needle. In this presentation, an angular encoder was used to track the 1-DOF rotational motion. The needle itself provides an A-line real-time feedback to user, so that the strong contrast from bone could be used for the warning to prevent the needle from collision. An ultrasound image of a slice of the scanning trajectory can be formed during the procedure, which can aid in determining the direction the needle should proceed.

For a practical workflow, the conventional blind insertion can be categorized into finding insertion, actual insertion, forward motion of the needle penetrating the subarachnoid space, and CSF collection. In our proposed workflow, our image/sensing guidance can take place at any intermediate step. First, the physician palpates the patient's back, as in the current standard of care. Once the initial entry point has been determined, the tracking holster is placed on the back of the patient at the determined location. When the holster is secured, the physician threads the needle through the holster into the patient. To generate an image, the physician sweeps the needle in an arc, a motion similar to one that is already needed in navigating the needle for a blind procedure. The adipose and connective tissues surrounding the spine are soft and they simply move out of the way of the needle while sweeping, so tissue damage is not a concern. This sweeping motion allows our system to collect data from both the needle probe and the tracking holster. As the algorithm processes this data, the image is updated on the screen for the physician to use in real-time. The physician is then able to sweep again at a deeper layer to produce another image. During the needle insertion, the distance from bone to the needle can be updated in real-time and the surrounding structures can be imaged by sweeping the needle at any time. In addition, the position of the needle within the image can be updated in real time from the encoder. After reaching the dura, the ultrasound element insert can be pulled out and a regular lumbar puncture atraumatic needle (22, 24 or 26G) threaded in to puncture the dura for CSF collection, creating a small hole in the dura and minimizing the possibility of iatrogenic complications arising. In this way, it is possible to safely perform a lumbar puncture while avoiding structures along the way to the subarachnoid space.

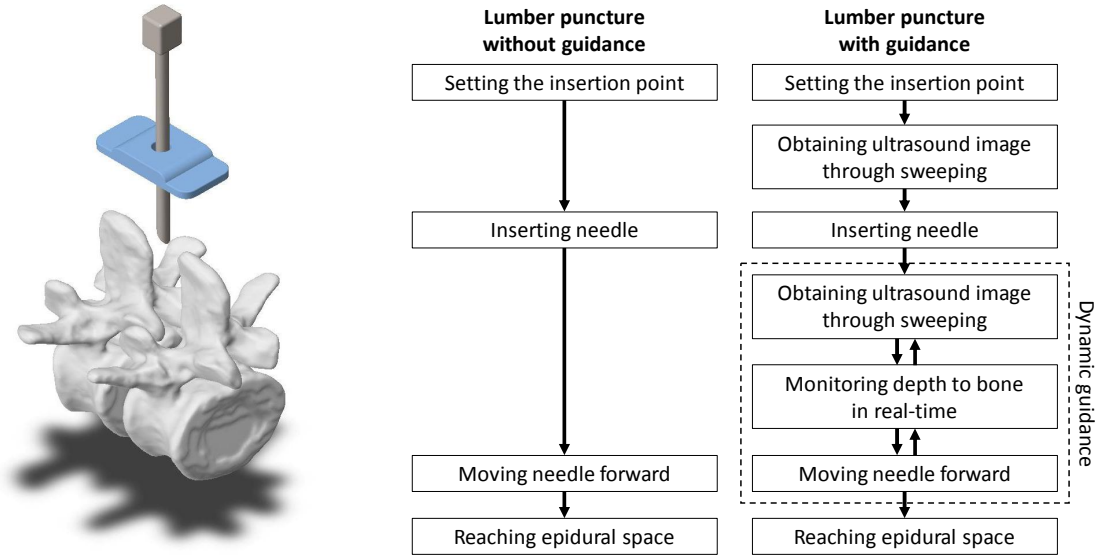

Fig. 2. The concept of the proposed system. (a) the illustration of the needle with respect to the spine. The blue piece of the attachment will guide (b) The workflow diagram of the blind needle insertion, compared with the proposed procedure with dynamic ultrasound guidance.

2.2 Ultrasound Tracking

The proposed imaging approach is based on the accurate tracking of the element location informed by a 12-bit absolute magnetic angular encoder (AEAT-6012). The encoder is able to provide absolute angle detection with a resolution of 0.0879º; it has no upper speed limit, though there will be fewer samples per revolution as the speed increases. The encoder is connected to an 'encoder-to-tube' adapter, which allows the pivot angle of the needle to directly correspond to the angle of read by the encoder. The current design incorporates an Arduino UNO which collects the encoder angle while an oscilloscope collects from the element itself.

2.3 Back Projection Based Synthetic Tracked Aperture Reconstruction

Utilizing rotation angle information, the synthetic aperture focusing is applied to reconstruct a 2D ultrasound image [15-18]. All rotation angle positions are accumulated and form a virtual ultrasound array with curvilinear scanning. The collected radio-frequency (RF) data are mapped into polar coordinates, and a back projection process is applied based on the virtual array. The relationship between pre and post reconstruction can be formulated as

$$y_{bf}(m,n) = \sum_{e} y_{bf_e}(m,n,e), \tag{1}$$

$$y_{bf}(m,n,e) = y_{pre}(d,e), \tag{2}$$

where ybf is the final reconstructed RF data, ybfe is the reconstructed RF data from single position, and ypre is the received raw RF data. *m*, *n* are the pixel information of the lateral and axial direction, respectively. The distance in the pre-beamformed data is *d,* and the received element number is *e*. The received signal distance is related to the actual image geometry from

$$d^2 = m^2 + n^2. \tag{3}$$

For each element position, this back projection is repeated. Figure 3 presents the process. From the very left, a single element back projection is shown. As the number of poses increases, the focusing point is gradually made and the point targets get smaller. When the very right image, in which symmetric information was used, each point target is reconstructed appropriately. Envelope detection and scan conversion are applied on the beamformed image, and the final STRATUS image is displayed in Cartesian coordinates.

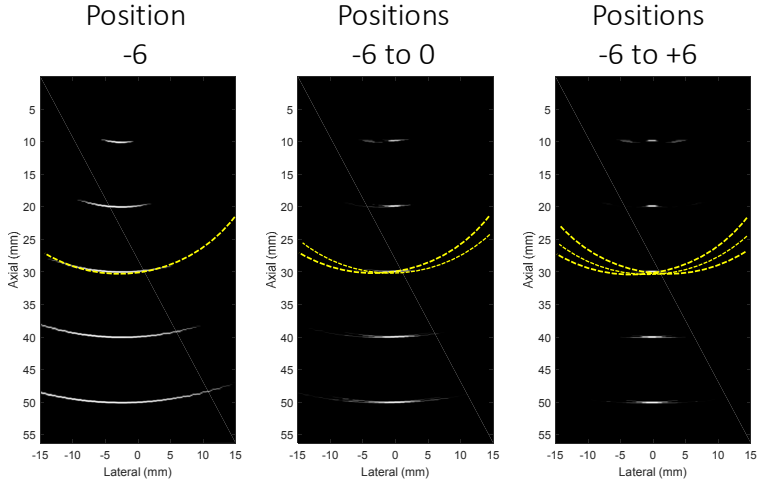

Fig. 3. The back projection reconstruction process corresponding poses. Left: A position -6 degree from the center pose was back-projected. Middle: Position in the range from -6 degree to 0 degree position were back-projected and summed. Right: Positions in the range from -6 degree to +6 degree position were back-projected and summed. The yellow line represents the back projection geometrical loci of the point at 30 mm depth point target.

3. METHODS

3.1 Simulation

Simulation was performed first to demonstrate the algorithm and observe the effect of errors. 5 point targets were simulated from 10 mm to 50 mm with 10 mm intervals. The sample frequency was 40 MHz, and center frequency of the point target was set to 4 MHz. The signals were received by a single element receiver which had a 40 mm rotation radius. The image was reconstructed with the back projection algorithm. 128 poses with 0.46 degree pitch were sampled by scanning the target field. Full-width at half maximum (FWHM) was used as the metric to represent the point target size as well as the lateral resolution.

3.2 Experimental Setup

As described in the section 2.1, the needle-shape ultrasound transducer is based on the PZT-5H element placed on the tip of the wire inserted in a 14G Quincke needle. The fabricated single element transducer is mounted on a holster with a rotation encoder to read precise rotational position [19]. The distance from the needle tip to the rotation pivot point was 36 mm. The transmission was triggered by a function generator, and received ultrasound and the trigger signals are captured by an oscilloscope or data acquisition system (US-Key, Lecoeur Electronique). In this validation experiment, we first scanned with a known trajectory. The top of the needle was attached to a Cartesian stage which was used to precisely rotate the needle and set its position, which allowed it to hold steady at each incremental angle step. The RF data was collected nine times at each position, and we used the averaged RF line at each position for synthetic image formation. For the freehand scanning, the needle was moved freely along the rotation, and data for 500 positions for ultrasound and rotation tracking were collected. The encoder and ultrasound reception was synchronized through MATLAB software. The ultrasound data is collected in real-time using a data acquisition (DAQ) device. The tracking data and the ultrasound data are transferred to a PC for data processing.

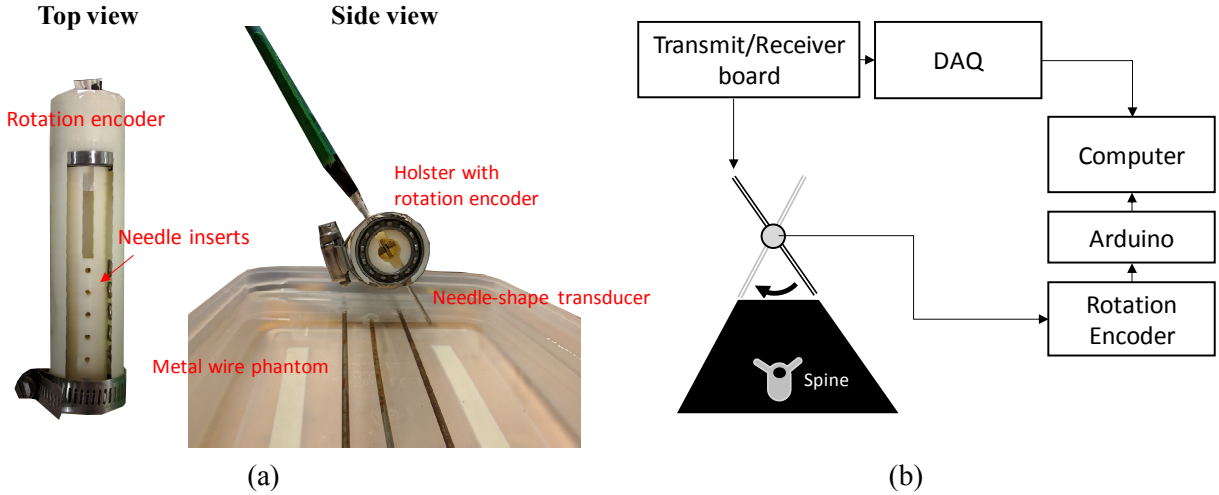

Fig. 4. Experimental setup. (a) The pictures of needle transducer mounted on the holster and the metal wire phantom design. (b) Diagram of hardware integration for the single element STRATUS system.

4. RESULTS

4.1 Simulation Results

The result of the simulated point targets is shown in Fig. 4. For the ground truth data, all points were reconstructed well. Two types of error sources were added to the data. The first type of error was axial error; this error could be introduced by tissue motion artifacts or the motion of the holster itself. The second type of error was the rotation reading error. If the rotation reading has an error or the recording was faster than the actual motion, this false reading could be sensed and cause distortion on the reconstructed image. As seen in Fig. 4 (b-c), the image quality was drastically worse compared to the case with no error.

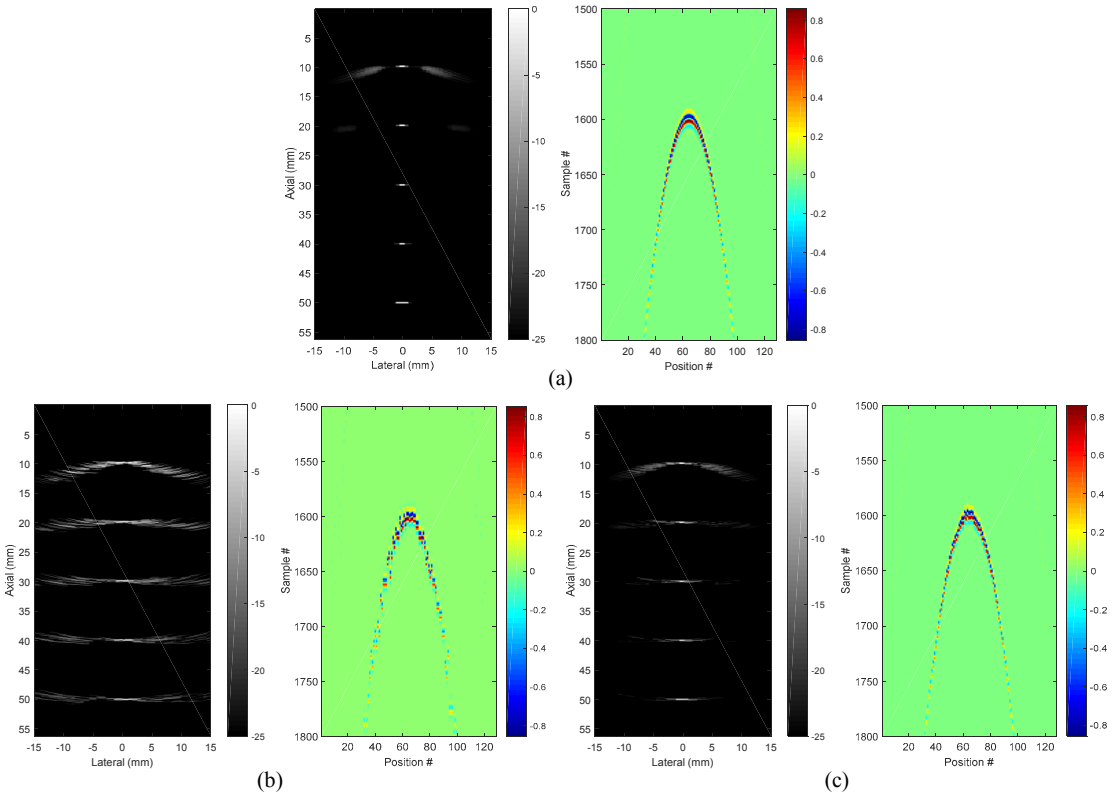

Fig. 5. Simulated point targets and corresponding received RF data of a point at 30 mm depth. (a) ground truth image with no error. (b) The result with error in the axial axis, and (c) the result with error in the rotation axis.

The next objective was to observe the change of image quality vs the magnitude of error. The error was introduced by shifting the pre-beamformed RF in axial and angle axis. Fig. 6 shows the FWHM for certain error conditions. The magnitude of the error represents the standard deviation of the randomized shift added to the data. For the axial motion, the resolution was stable until 0.04 mm but suddenly became unstable from 0.05 mm on. For angle error, the error was acceptable until 1 degree but gradually reduced the image quality. If these errors are inevitable, then it is necessary either to sweep the same region several times to average out the error or to sample angles in smaller steps to mitigate the effect of error. Sweeping at a lower speed is another solution, but there is a trade-off because slow sweeping may permit errors due to breathing or body motion.

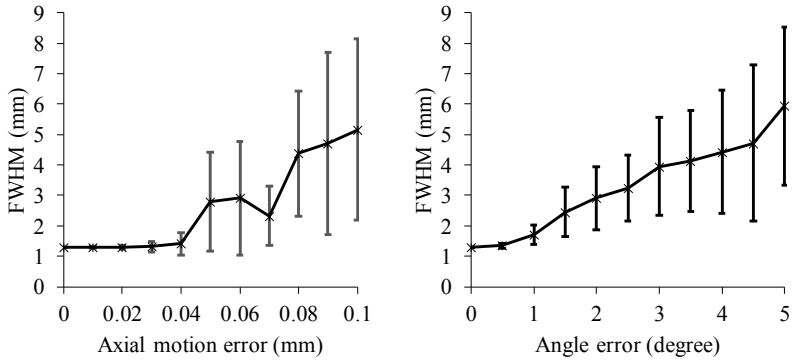

Fig. 6. The full-width at the half maximum (FWHM) of the point targets for various errors and the magnitude of image degradation as the error increases. (a) The resolution when error is introduced in the axial direction for each receive line. (b) The resolution when error in introduced in the rotation direction.

4.2 Needle Sensing Evaluation

Before moving to the image formation, we confirmed the sensitivity of the depth detection, and the accuracy of the rotation encoder (Fig. 7). The depth calibration result is shown in Fig. 7(a), which presents the needle could accurately sense the depth information with our fabricated transducer. The needle depth sensing itself could be used as a real-time guidance tool, by indicating how deep the needle could go before hitting the object. This could work well, given that in our case, the largest structures are bone, and the segmentation should be possible by comparing the signal from other soft tissues. The angle sensitivity of the needle was 11.44 degrees where -6 dB signal strength was reached. The accuracy of the encoder was assessed experimentally prior to implementing in our system. The needle was placed vertically and incrementally rotated such that, at each new angle position, the new angular reading from the encoder and the horizontal displacement of the tip of the needle were recorded. With the horizontal displacement of the needle tip (x) and the known length of the arc radius (r), the actual angle can be calculated with the simple trigonometric identity:

$$\theta = \tan^{-1}\frac{x}{r}. \tag{4}$$

This was compared to the angle found with the encoder to find the error, and a linear trend was observed as seen in Fig. 7(b). These two pieces of information indicate that the sensing system is sufficient to produce a image with minimal distortion as indicated by motion from tissue or sensors.

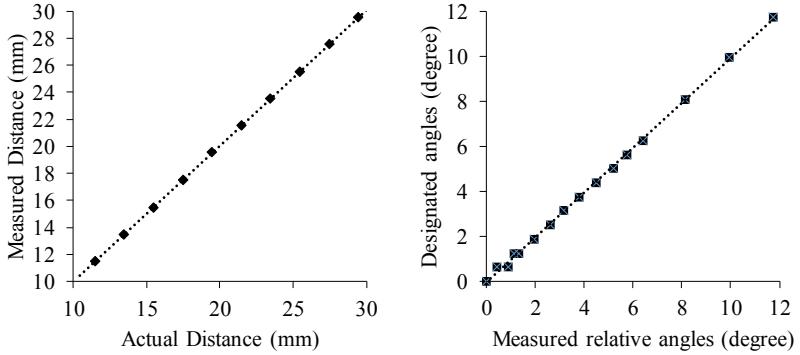

Fig. 7. The evaluation results of the needle (a) and the rotation encoder (b). (a) The distance from the needle reading was compared to the designated motion distance, and (b) the angle measurement for the encoder was compared to the actual angle. The correlation function for both the depth sensing and rotation encoder sensing was higher than 99.99 and 99.94%, respectively.

4.3 Single Element STRATUS Imaging with Controlled Scan

Experimental results are shown in Fig. 4. The original signals contain strong electrical artifacts, which were minimized by subtracting a RF line with no target. Although the background noise was strong, the target signals were seen in the RF line (Fig. 4a). The center frequency of the received target signals was 10 MHz. Figure 4b shows the reconstructed images before and after applying synthetic aperture focusing (SAF) on the same data set. The point target in the pre-beamformed data did not appear across a wide range of angles, because the needle has inherent high anglular sensitivity. Ideally, a wider beamforming aperture size should be used as the focusing depth becomes deeper. The beamformed image shows a clear resolution improvement for all targets, but the targets' contrasts were slightly deteriorated because of the strong background noise and off-axis summation from tracking errors. The beamforming side lobes appeared in the near field, which could be attributed to incoherency of the data due to the tracking inaccuracy. The FWHM of the shallower wire improved from 3.53 mm to 1.94 mm through SAF, and that of the deeper wire improved from 6.36 mm to 2.51 mm.

After the system was tested with point targets, the real spine bone phantom was then scanned to observe and test a more practical implementation. Fig. 8 shows the image of the spine in the slice crossing the vertebrae horizontally. While two edges of the bone were observed, the center region captures the bone in the middle, signifying that this point should be avoided for insertion. The contrast is still not fully obvious but this could be due to the angled reflection from the bone. When the needle angle and the target are perpendicular, the signal will reflect mostly to the receiver but if there is an

angle, the reflection will be not as strong as the perpendicular position. Thus, the contrast should not be the main focus of the approach.

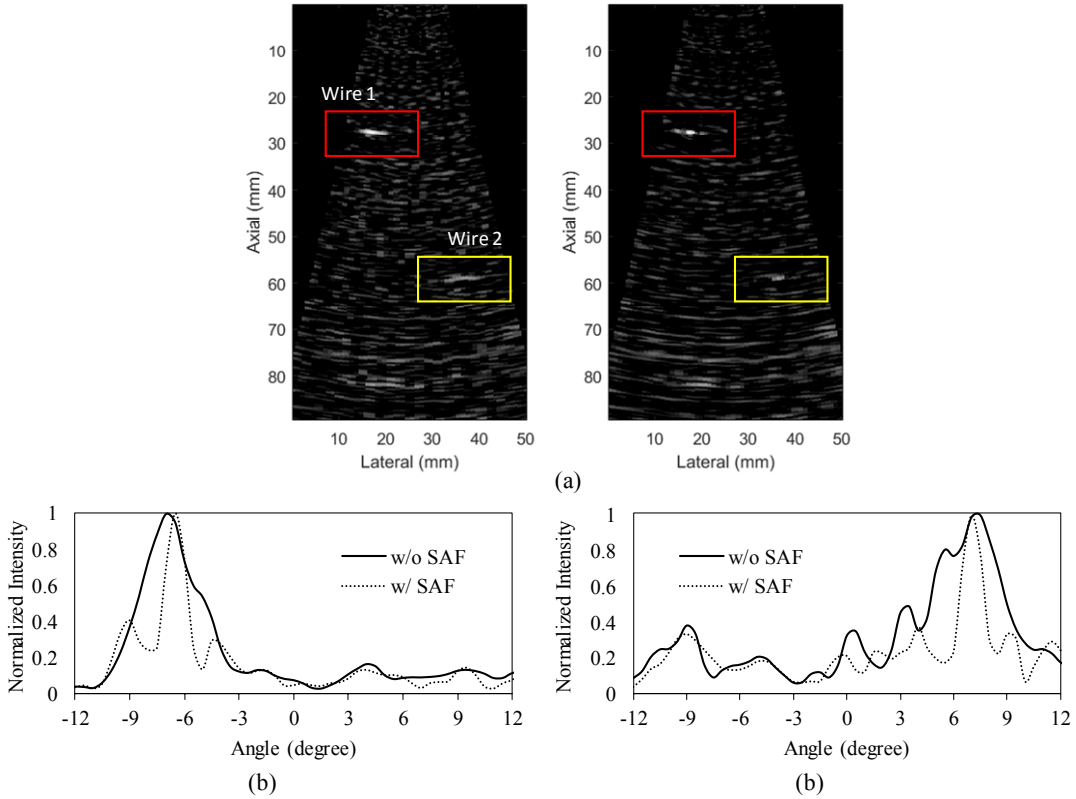

Fig. 8. The imaging result of the metal wire phantom. (a) The B-mode image of pre- and post-beamforming. The angle axis profiles of two metal wire targets are shown in (b) and (c), corresponding to wire 1 and 2, respectively. For each profile, the results before and after applying synthetic aperture reconstruction are compared.

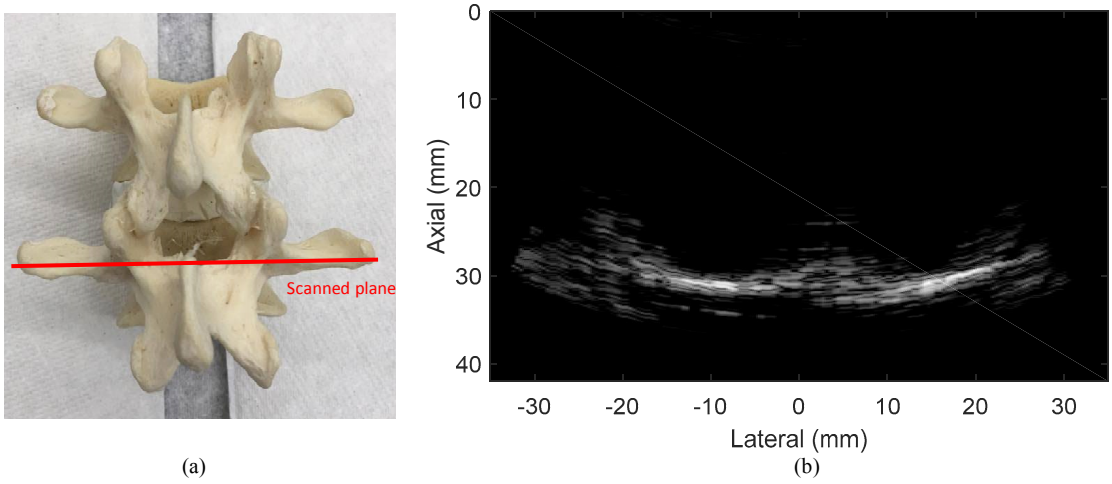

Fig. 9. (a) The spine phantom picture and the scanned plane. (b) The STRATUS image of the spine phantom. The contrast from the center region indicates that the needle cannot go through without changing the insertion orientation.

4.4 Single Element STRATUS Imaging with Free-hand Scan

Although previous results are based on fixed motion, we also tested the feasibility of free hand scanning with the same wire phantom. 500 positions were recorded by sweeping the needle back and forth, and at the same time, the rotation angle was collected by the encoder. The angular range of the scanning was 61 degrees. The result captures the three wire targets well, and the size and position match the original phantom design. Comparing the reconstructed point size of the very left wire, the FWHM improved from 2.08 mm to 0.95 mm through synthetic aperture beamforming.

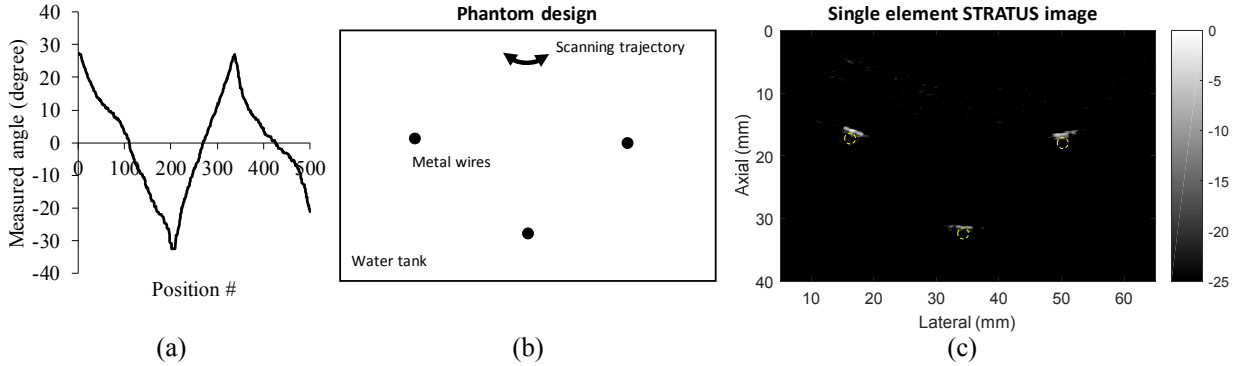

Fig. 10. The freehand scanning result of single element STRATUS imaging system. (a) The measured angle for 500 needle positions. (b) The metal wire phantom design, and (c) the STRATUS image from the data of 500 positions corresponding to 61 degrees sweeping.

5. DISCUSSION AND CONCLUSIONS

The current standard of care for LPs introduces a wide range of iatrogenic complications and places a heavy burden on the patient, physician, and healthcare system overall. The proposed imaging system incorporates an ultrasound element at the tip of the needle to allow for high resolution imaging. The needle probe bypasses the attenuation from adipose tissue and skin that plagues traditional ultrasound at greater depths. By providing the physician with visualization of the tissue ahead, the system can reduce complications and improve patient outlook by allowing the physician to correctly guide the needle to the subarachnoid space and avoid peripheral structures such as bone. The simulation validation and experiments using our prototype successfully demonstrate the potential of the tool for lumbar punctures guidance.

Compared to other imaging systems, there are clear advantages. Unlike other ultrasound guidance systems, the proposed system is an independent imager that does not require any registration process which could introduce additional needle tracking inaccuracy. The real-time sensing information is the most direct and informative means to prevent undesired contact between the needle and bone. As the image plane is kept to be in the needle frame, there is no out-of-plane error which could be introduced due to ultrasound beam thickness in the conventional ultrasound probe based guidance. The system also requires minimal electrical components, making it more cost effective.

Another unique aspect of the system is the fact that the proposed system could update the sensing/imaging at any intermediate insertion depth in real-time, while conventional guidance has to rely on information from prior to entry such as preoperative CT or ultrasound-to-tool calibration. This up-to-date information not only makes the information more reliable, but also facilitates higher resolution especially as the needle approaches the real target. Conventional ultrasound could have a limited imaging depth depending on the object and frequency used which is more of an issue in obese patients, the very group in which image guidance is critical. Thus the proposed system can provide clearer and more precise information for guidance.

Regarding the limitation of the system in practical implementations, the tissue layer could cause signal attenuation that lowers the intensity from the bone surface. Therefore, a more sensitive receiver circuit and needle are desired. SNR can be improved by electrical impedance matching between the sampling circuit and needle. Another solution is to use a PZT element with lower center frequency, which can lower the requirement for the error because the wavelength will also be lower. This will also help reduce beamforming artifacts because the wavelength of signals becomes longer. Other than that, signal processing or a more adaptive beamforming algorithm could also help to counter this concern. The

tracking accuracy due to motion artifacts are considered as another problem. There is some inevitable error from the mis-synchronization between the tracking and the ultrasound data. Ideally, the tracker should be fast enough to reduce the error introduced. Other than that, unexpected angular sensitivity from a non-orthogonal element (i.e. an element that was placed at a tilt from the manual fabrication process) could introduce beamforming error.

Future works include building an adaptive image formation algorithm taking into account the known angular sensitivity, and enhancing the SNR of the image. The system will be further tested in the more realistic environments such as *ex vivo* tissue or *in vivo*.

ACKNOWLEDGEMENT

The authors would like to acknowledge Shayan Roychoudhury for help creating a figure, and Larissa Chan, Ernest Scalabrin, Suraj Shah, Arden Chew, Kush Gupta for their contributions to the project in a variety of capacities. The authors also acknowledge VentureWell and the Coulter Translational Foundation for their support throughout this project.

REFERENCES

[1] Armon C., Evans R. W., "Addendum to assessment: prevention of post-lumbar puncture headaches," Neurology 65, 510-512 (2005).
[2] American Society for Healthcare Risk Management, "Risk Management Handbook for Health Care Organizations", Jossey-Bass, 5 (2009).
[3] Edwards C., Leira E. C., and Gonzalez-Alegre P., "Residency Training: A Failed Lumbar Puncture Is More about Obesity than Lack of Ability," Neurology 84(10), e69-72 (2015).
[4] Shah K. H., Richard K. M., et al., "Incidence of traumatic lumbar puncture," Academic Emergency Medicine 10(2), 151-4 (2003).
[5] Ahmed S. V., Jayawarna C., and Jude E., "Post lumbar puncture headache: Diagnosis and management," Postgraduate Medical Journal 82(273), 713-716 (2006).
[6] Shaikh F., Brzezinski J., Alexander S., Arzola C., Carvalho J. C., Beyene J., and Sung L., "Ultrasound imaging for lumbar punctures and epidural catheterisations: systematic review and meta-analysis," BMJ 346 (2013).
[7] Brook A. D., Burns J., Dauer E., Schoendfeld A. H., and Miller T. S., "Comparison of CT and Fluoroscopic Guidance for Lumbar Puncture in an Obese Population with Prior Failed Unguided Attempt," Journal of NeuroInterventional Surgery 323-27 (2013).
[8] Engedal T. S., Ørding H., Vilholm O. J., "Changing the needle for lumbar punctures," Clinical Neurology and Neurosurgery 130, 74-79 (2015).
[9] Tamas U., Abolmaesumi P., Jalal R., Welch M., Ayukawa I., Nagpal S., Lasso A., Jaeger M., Borschneck D., Fichtinger G., and Mousavi P., "Spinal Needle Navigation by Tracked Ultrasound Snapshots," IEEE Transactions on Biomedical Engineering 59(10), 2766-72 (2012).
[10] Moore J., Clarke C., Bainbridge D., Wedlake C., Wiles A., Pace D., and Peters T., "Image Guidance for Spinal Facet Injections Using Tracked Ultrasound," Medical Image Computing and Computer-Assisted Intervention, (2009).
[11] Chen E. C. S., Mousavi P., Gill S., Fichtinger G., Abolmaesumi P., "Ultrasound guided spine needle insertion," Proc. SPIE 7625, 762538 (2010).
[12] Najafi M., Abolmaesumi P., Rohling R., "Single-Camera Closed-Form Real-Time Needle Tracking for Ultrasound-Guided Needle Insertion," Ultrasound in Medicine and Biology, 41(10), 2663-2676 (2015).
[13] Wang X. L., Stolka P. J., Boctor E., Hager G., Choti M., "The Kinect as an interventional tracking system," Proc. SPIE 8316, 83160U (2012).
[14] Nagpal S., Abolmaesumi P., Rasoulian A., et al., "A multi-vertebrae CT to US registration of the lumbar spine in clinical data," Int. J. CARS 10(9), 1371-81 (2015).
[15] Jensen J. A., Nikolov S. I., Gammelmark K. L., Pedersen M. H., "Synthetic aperture ultrasound imaging," Ultrasonics 44(22), e5-e15 (2006).
[16] Zhang H. K., Cheng A., Bottenus N., Guo X., Trahey G. E., Boctor E. M., "Synthetic Tracked Aperture Ultrasound (STRATUS) Imaging: Design, Simulation, and Experimental Evaluation," Journal of Medical Imaging 3(2), 027001 (2016).

[17] Bottenus N., Long W., Zhang H. K., Jakovljevic M., Bradway D. P., Boctor E. M., Trahey G. E., "Feasibility of Swept Synthetic Aperture Ultrasound Imaging," IEEE Transactions on Medical Imaging 35(7), 1676-1685 (2016).
[18] Zhang H. K., Finocchi R., Apkarian K., Boctor E. M., "Co-Robotic Synthetic Tracked Aperture Ultrasound Imaging with Cross-Correlation Based Dynamic Error Compensation and Virtual Fixture Control," Proc. IEEE International Ultrasonics Symposium (IUS), 1-4 (2016).
[19] Kim Y., Guo X., Boctor E. M., "New platform for evaluating ultrasound-guided interventional technologies," Proc. SPIE 9790, 97901J, (2016).